LAMINARIZATION OF MICRO-BUBBLE CONTAINING MILKY BUBBLY FLOW IN A PIPE

Akimi Serizawa[1], Tomohiko Inui[1], Toshihiko Yahiro[2], Zensaku Kawara[1]

1: Department of Nuclear Engineering, Kyoto University, Yoshida-Honmachi, Kyoto 606-8501, Japan
Phone & Fax: +81-75-753-5829, E-mail: E-mail: serizawa@nucleng.kyoto-u.ac.jp,
2: Aura Tec Co., Ltd, 1725-2, Tsubuku-Honmachi, Kurume, Fukuoka 830-0047, Japan
Phone: +81-942-32-2504, Fax: +81-942-38-3806, E-mail: yahiro@kumin.ne.jp

ABSTRACT

Micro bubble technology has become to attract people's concerns due to its wide potential in practical applications to a variety of advanced and conventional science and technologies. However, our knowledge of micro bubbles containing bubbly two-phase flow is almost nothing. We developed a specially designed nozzle which generates high intensity micro air bubbles (mean diameter~ 40microns, number density more than 2×10^5/cc). Using this micro-bubble generator, we carried out, as a first step, a measurement of two-phase frictional pressure drop, cross-sectional average void fraction and liquid velocity profiles. The measurement of local void fraction is underway. The range of average void fraction was up to 0.6 % which is enough to realize milky bubbly flow. The most exciting result we found is that the two-phase flow becomes laminarized by injecting such ultra small bubbles into the water flow. For 0.3~0.5% void fraction, laminar-turbulent transition occurred at Re=10,000~20,000. The cross sectional averaged void fraction does not follow a homogeneous flow model, and radial liquid velocity profile was a little bit flattened. The mechanism of flow laminarization and flow structures are now being pursued.

1. INTRODUCTION

Practical applications of micro bubble technology have recently become to attract people's great concerns in wide variety of areas in advanced and conventional science and technologies, such as energy conversion and heat removal devices, diagnosis by ultrasound echo due to micro bubble collapse, drug delivery systems, cleaning and sterilization by shock waves due to the collapse of high pressure micro bubbles, production of ozone water, mining using physical absorption at gas-liquid interfaces, purification and improvement of oil-contaminated soil and polluted water by air supply (sea, lake, river etc), absorption of carbon dioxide gas, fish culture, etc. Here, the micro bubbles may be defined as the bubbles with diameters of the order of less than several tens microns, since these sizes of bubbles exhibit in fact somehow different behaviors from those observed with ordinary sized bubbles in their chemical and physical aspects.

Up to now, much attention has been focused merely on the application of micro bubble technology and methods of micro bubble generation. Hydro-dynamic behaviors of micro bubbles containing two-phase flow unfortunately received much less attentions. For example, our current understanding of turbulent structure of bubbly two-phase flow is limited to the flows where the size of bubbles in the flow generally stands between the integrated turbulent scale and micro turbulent scale, as indicated in Figs.1 and 2 (Michiyoshi & Serizawa [1]). The size of micro bubbles is however smaller than micro turbulent scale. It is therefore anticipated that the bubbles with diameter smaller than the micro turbulent scale may exhibit different behaviors from those shown by ordinary sized

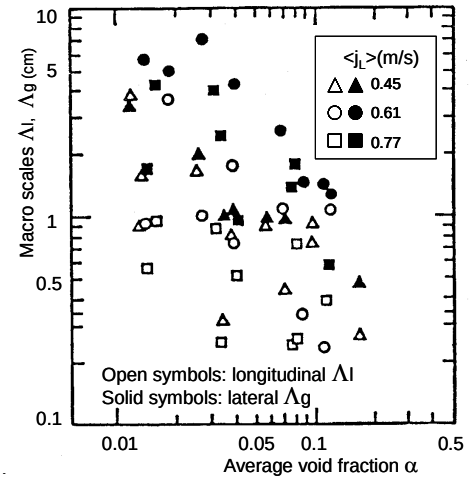

Figure 1 Macro Scale of Turbulence [1]

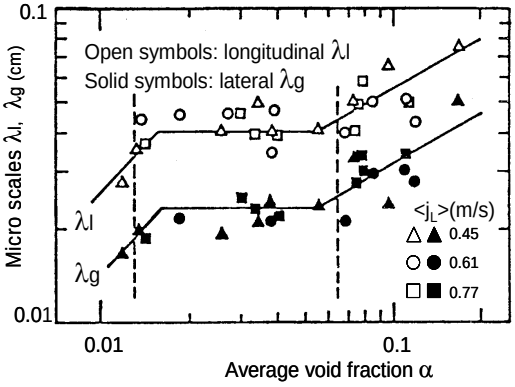

Figure 2 Micro Scale of Turbulence [1]

bubbles, specifically in the way of hydrodynamic interactions with the flow and thus the two-phase flow structures may be changed, as suggested by Fig.3 (Serizawa & Kataoka [2]). With this in mind, we aim at clarifying turbulent structures of air-water milky bubbly flow in a pipe which contains very fine bubbles of the order more or less 50 microns.

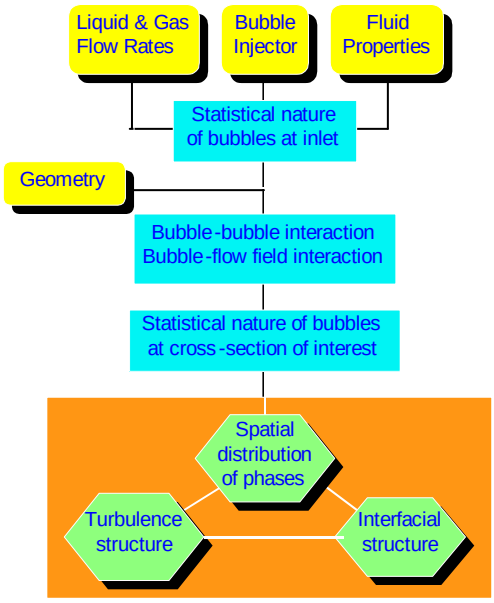

Figure 3 Flow Chart of Bubbly Flow Development

2. WHAT IS A MICRO BUBBLE AND HOW TO MAKE MICRO BUBBLES

2.1 Bubble behavior

Micro bubbles with diameters smaller than several tens microns are supposed to have the following features:
(1) large interfacial area concentration for given void fraction.
(2) very low rise velocity-long residual time in liquid phase
(3) very low possibility of bubble coalescence-good dispersion character and mixture homogeneity
(4) dissolving character into liquid – bubble life (depending on the method of micro bubble generation)
(5) low electrical potential – good for physiological activation
(6) physicochemical properties
(7) acoustic properties
(8) fluid dynamic properties – reduction in skin friction, etc
(9) others

As stated earlier, our concerns are focused on
(1) what are bubble-turbulence eddy interactions ?
(2) what are bubble-bubble interactions ?
Based on a visual observation using a microscope, we found that micro bubbles behave like solid particles without significant shape deformation when they collide to each other (Fukami [3]). A series of pictures showing this are demonstrated in Fig.4. From this finding, we speculated on the micro bubble motions by numerical experiment, and we came to a hypothetical bubble-bubble interaction force model which considers the effects of two major forces acting on two micro bubbles approaching to each other (Matsumoto et al.[4]). These forces are working in an opposite direction to each other, in attracting and repulsing directions, respectively, depending on the distance between the two approaching micro bubbles

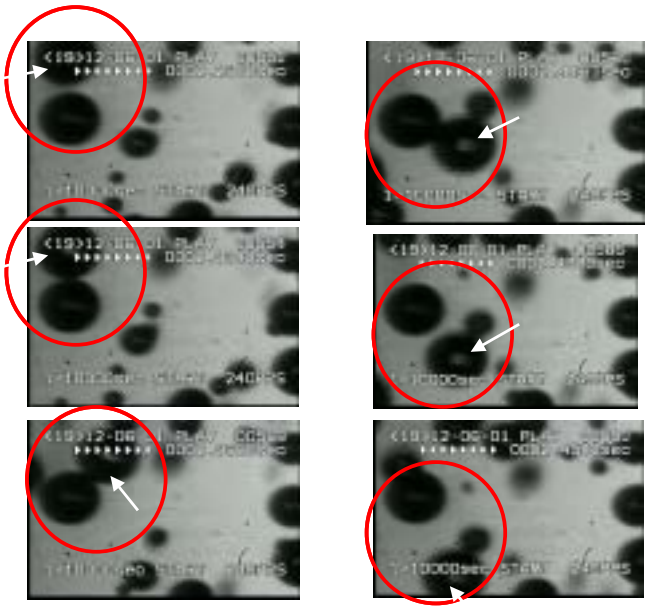

Figure 4 Collision of Two Micro Bubbles (~50microns)

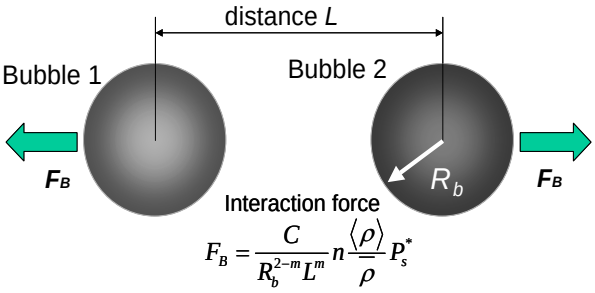

Figure 5 bubble-Bubble Interaction Model [4]

(see Fig.5), and are given by Esq. (1) and (2).

$$F_B(x_s) = \frac{C_1}{L^2} n \frac{\langle \rho \rangle}{\rho} P_s^* \qquad (\text{for } L \le 5R) \tag{1}$$

$$F_B(x_s) = \frac{C_2}{LR_b} n \frac{\langle \rho \rangle}{\rho} P_s^* \qquad (\text{for } L > 5R) \tag{2}$$

where R_b, L and x_s are radius of micro bubbles, the distance between two adjacent micro bubbles and surface position, respectively. C_1 and C_2 are constants and $n(x_s)$ is a normal vector to the surface at x_s. Here,

$$\langle \rho \rangle = \sum_m F_m \rho_m \tag{3}$$

$$\overline{\rho} = (\rho_1 + \rho_2)/2 \tag{4}$$

and F_m and ρ_m are volume fraction and density of the i-th phase, respectively. P_s^* is the surface pressure based on the bubble radius R_b.

These forces appear in the momentum equation with the CSF (Continuum Surface Force) model [5] in the interface tracking solver MARS [6] as

$$\frac{\partial \mathbf{u}}{\partial t} + (\mathbf{u}\cdot\nabla)\mathbf{u} = G - \frac{1}{\langle\rho\rangle}\left(\nabla P + \nabla\cdot\tau - F_{v,total}\right) \qquad (5)$$

where the operator $\langle\ \rangle$ represents a spatial averaging.

The total surface tension force $F_{v,total}$ at the certain surface position x_s can be expressed as:

$$F_{v,total} = F_v(x_s) + F_B(x_s) \qquad (6)$$

where the nominal surface tension force based CSF model is given by

$$F_V(x_s) = \sigma\kappa(x_s)\,n(x_s)\frac{\langle\rho\rangle}{\bar{\rho}} \qquad (7)$$

where the surface curvature at x_s, $\kappa(x_s)$, is obtained by unit normal vector calculated from the F values of surrounding cells as follows:

$$\kappa = \frac{1}{|n|}\left[\left(\frac{n}{|n|}\cdot\nabla\right)|n| - (\nabla\cdot n)\right] \qquad (8)$$

Here, $|n|$ is the norm of $\mathbf{n}$.

It is thus assumed in this model that the interaction forces act on the bubbles in two different ranges: the long range $(L > 5R_b)$ (attracting force) and the short range $(L \le 5R_b)$ (repulsion force). In the short range, the interaction force works like a Coulomb force resulting from a dipole moment at surfaces, proportional to L^{-2}. Whereas in the longer range, this force is interpreted as a non-local force like a force originating from pressure propagation caused by rapid change of the bubble shape, i.e., resulting from the effect of liquid compressibility due to pressure waves caused by interface deformation of neighboring bubbles. This force is supposed to be related to thermodynamic processes for the surface excess energy at the interface and thus proportional to surface curvature of the bubbles (~$1/R_b$). Although these forces are not validated theoretically yet, this bubble interaction force model predicts well the bubble-bubble interaction as shown in Fig.6.

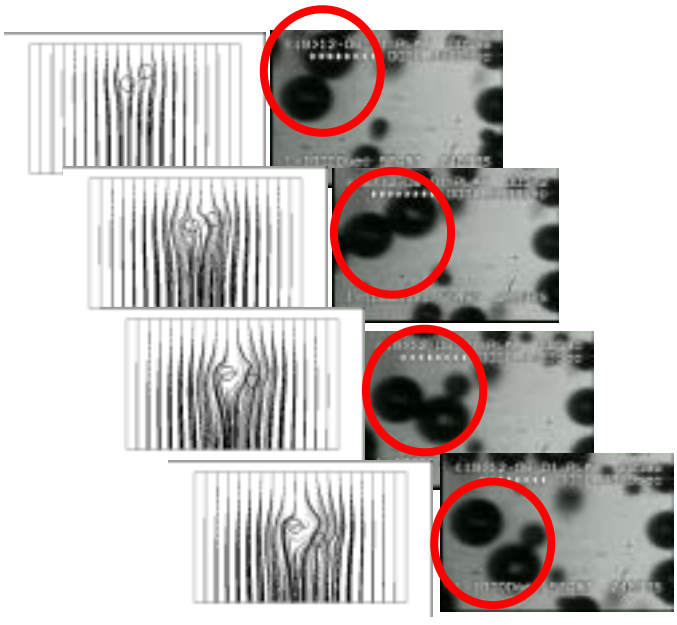

Figure 6 Comparison between Prediction and Observation

2.2 Methods of micro bubble generation

There are so many methods of micro bubble generation so far proposed. In general, all of the existing or proposed methods use a combination of either two or three among depressurize-ation of air-saturated water, bubble break-up by shear force and cavitation. Some of the typical examples are shown in Fig.7. We tested all of these devices and others by computer-aided visual observation of micro bubble diameter distributions (Serizawa et al.[7]). We eventually came to a conclusion that our developed device "cavitation nozzle" showed the best operational performance in terms of the mean bubble diameter, standard deviation in bubble size distribution and bubble number density (Fig.8).

A question is raised as to the maximum void fraction attained with various methods of bubble generation. Small bubble number density of micro bubbles results in low void

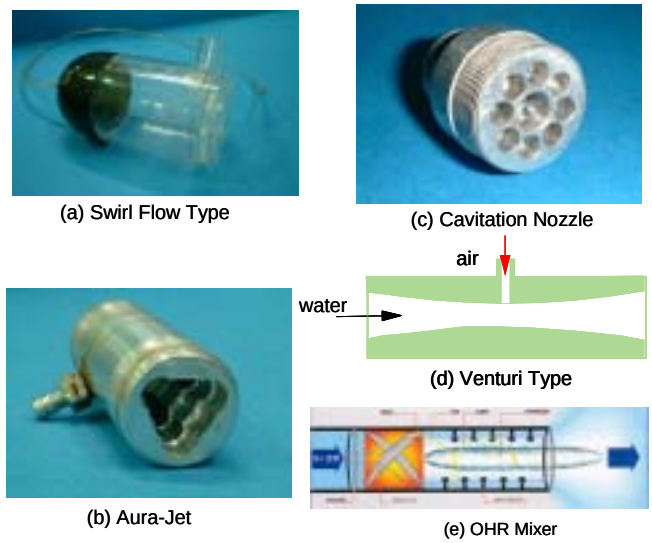

Figure 7 Various Designs of Micro Bubble Generation

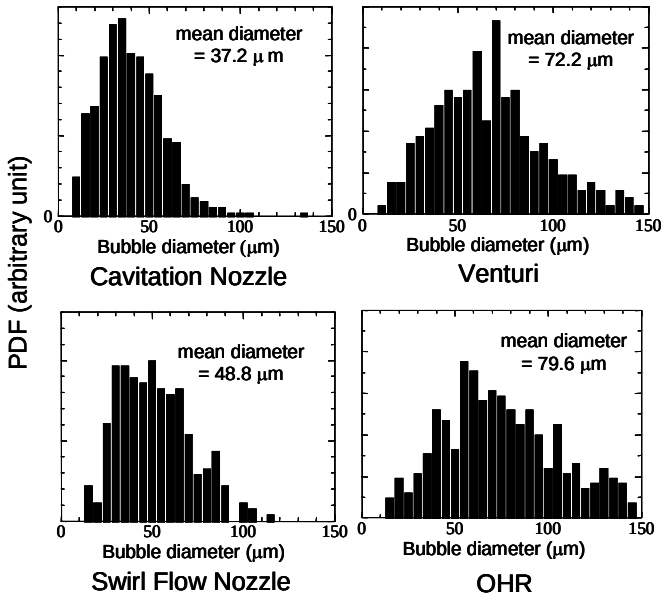

Figure 8 Bubble Size Distribution with Different Devices

fraction, and thus we cannot realize milky bubbly flow in a flowing system. Figure 9 shows a diagram of bubble diameter (μm) *versus* bubble number density (bubbles/cm^3) obtained by conventional bubble generation methods [8]. Figure 10 shows the maximum void fraction estimated from the envelop shown in Fig.9 [9].

After a long struggle with high density micro bubble generation methods, we found that our developed cavitation nozzle successfully satisfies the requirements for beautiful milky bubbly flow in a pipe, giving up to 0.6% void fraction for a wide range of liquid velocity condition (Fig.11).

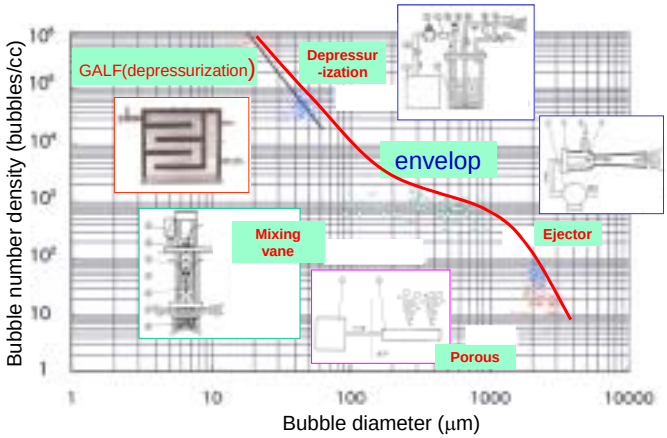

Figure 9 Bubble Diameter *versus* Bubble Number Density [8]

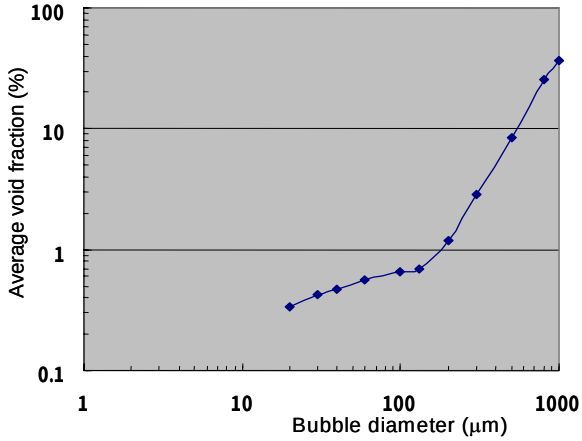

Figure 10 Maximum Void Fraction *versus* Bubble Diameter

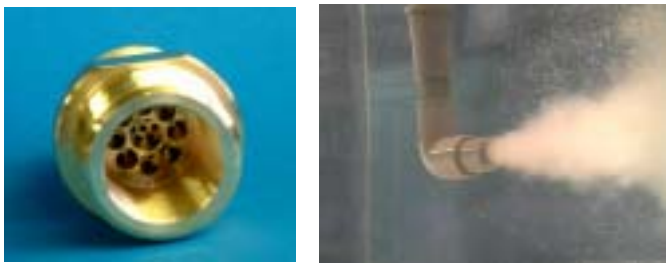

Figure11 Cavitation Nozzle and Micro Bubble Generation

3. EXPERIMENTAL APPARATUS

Figure 12 shows a schematic of air-water test loop used in the present work. The working fluids are deionized water and the air supplied from a gas bottle. The air flow was adjusted at the desired values by a flow control valve, and was sucked into the water flow through a venturi-type nozzle equipped at a downcomer just before a high-pressure pump. The air dissolves partially into the water flow and is depressurized by a micro bubble generator nozzle to form micro bubbles containing milky bubbly flow along with cavitation bubbles. The mean diameter of micro bubbles is roughly 40 μm throughout measurements with a negligible change of bubble size along the flow direction. The water flow in the test section was adjusted mainly by a bypath flow to keep the void fraction at a constant value irrespective of liquid flow rates. The micro air bubbles are separated from the water at the top of the test section by using three-stage swirl flow-type separator which is our original design (Fig.13).

The test section is a 4m long transparent acrylic circular pipe with 20 mm in inner diameter. We measured two-phase frictional pressure drop by using a monometer over a 1m long distance starting at roughly 2m downstream of the micro bubble generation nozzle. The cross-sectional average void fraction was precisely measured by two-phase mixture mass which was sampled in a 500 cc bottle submerged in a sampling tank equipped at the exit of the test section. The sampled mixture mass is measured by a high-precision electronic balance. The accuracy of void fraction measurement ($\Delta\alpha/\alpha$) was within about ± 5%. The local liquid velocity profile in radial direction was measured at a 3m elevation from the micro bubble generation nozzle with a calibrated Pitot tube based on a continuous squeeze model given by the following equation.

$$u = k\sqrt{\frac{\Delta p_k}{\rho(1-\alpha^2)}} \tag{9}$$

where u, k, Δp_k, α and ρ are liquid velocity, calibration

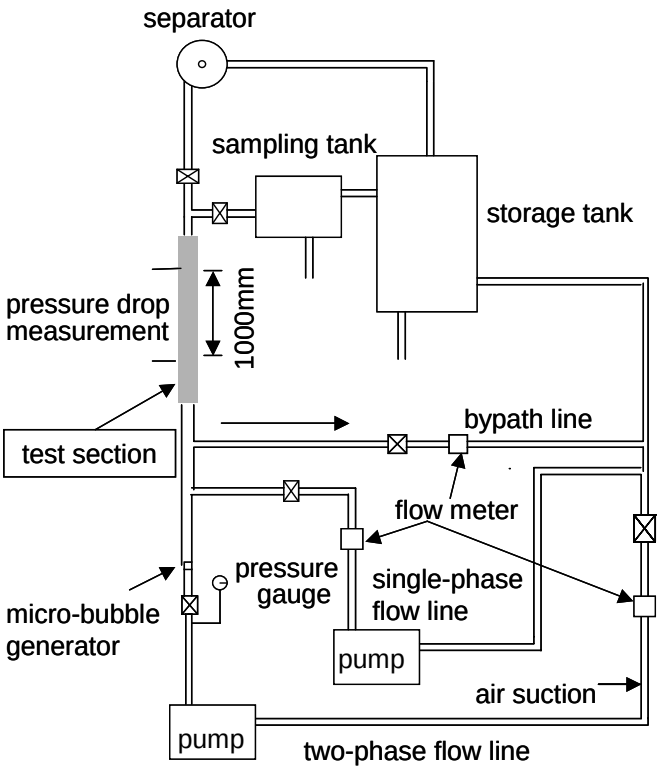

Figure 12 A Schematic of Two-Phase Flow Test Loop

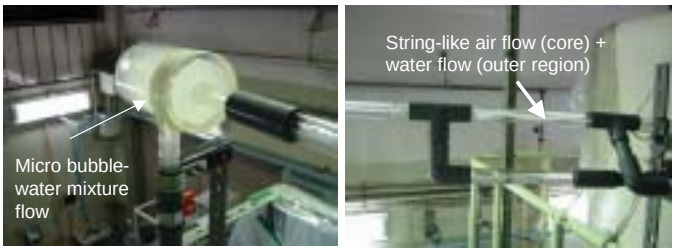

Figure 13 Micro Bubble-Water Separation

coefficient of the Pitot tube, measured dynamic pressure, local void fraction and liquid density, respectively. The local void fraction measurement within good accuracy is a very difficult job, since the order of magnitude of void fraction is more or less 0.1~0.6%. We are now trying to carry out local void fraction measurement by using a sampling probe method.

4. EXPERIMENTAL RESULTS AND DISCUSSIONS

4.1 Cross-sectional average void fraction

Figure 14 shows the measured void fraction $\langle\alpha\rangle$ against volumetric air flow ratio β. Contradictorily to our intuition, the experimental evidence suggests that the cross-sectional average void fraction follows a slip flow model with slip ratio S = 1.4, that is,

$$\langle\alpha\rangle = 0.702\beta \tag{10}$$

This equation is equivalent to a drift flux model equation with the distribution parameter C_0 = 1.42 and negligible void-weighted area-averaged drift velocity. Let us assume the following exponential laws for local void fraction and total flux distributions, where α, j, r and R are local void fraction, local total volumetric flux (= $j_L + j_G$) (the suffix L: liquid ,

$$j/j_c = 1-\left(r/R\right)^m \tag{11}$$

$$\frac{\alpha-\alpha_w}{\alpha_c-\alpha_w} = 1-\left(r/R\right)^n \tag{12}$$

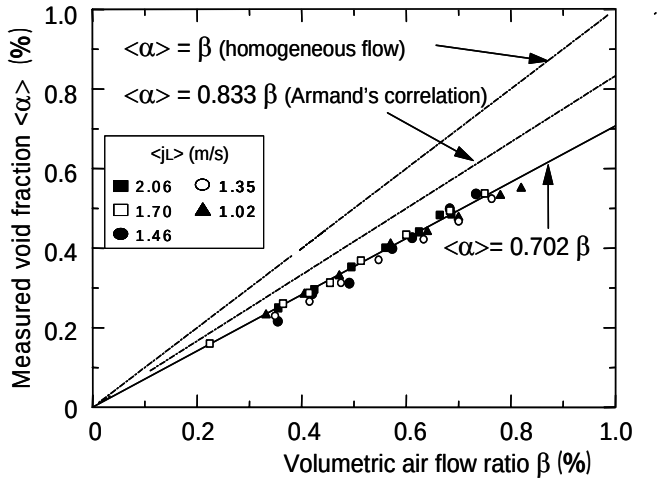

Figure 14 Void Fraction Measurement

G:gas), radial position and tube radius, respectively. The suffixes c and w represent the values at tube center and at the wall, respectively. The exponents m and n are experimentally determined constants. Then, we have the following equation for the distribution parameter C_0.

$$C_0 = \frac{\langle\alpha j\rangle}{\langle\alpha\rangle\langle j\rangle} = 1+\frac{2}{m+n+2}\left(1-\frac{\alpha_w}{\langle\alpha\rangle}\right) \tag{13}$$

For uniform void fraction distributions, we have $\langle\alpha\rangle = \alpha_w$ and n=0, irrespective of the value of the void fraction. Then, Eq.(13) yields to

$$C_0 = 1 \tag{14}$$

Eq. (14) can be of course obtained straightforward from the definition of C_o as well. From this argument, the experimentally observed value of C_0 = 1.42 is never consistent with uniform void distribution whatever the liquid velocity distribution is. To make clear the reason, we have to measure the phase distribution profiles.

4.2 Two-phase frictional pressure drop

In view of the negligibly small quality (gas content) of micro bubbles containing milky bubbly flow, we may well define the two-phase friction factor f_m and the two-phase Reynolds number Re in the same way for single-phase flow:

$$\frac{\Delta P_f}{l} = f_m\frac{\rho\langle j_L\rangle^2}{2D} \tag{15}$$

$$\mathrm{Re} = \frac{\rho\langle j_L\rangle D}{\mu} \tag{16}$$

where ΔP_f, l and μ are frictional pressure drop over the length l, the distance between the two pressure taps and liquid viscosity, respectively.

Figure 15 represents the measured two-phase friction factor *versus* the two-phase Reynolds number diagram. Here the friction factors in laminar and turbulent flows given by the following equations are referred to.

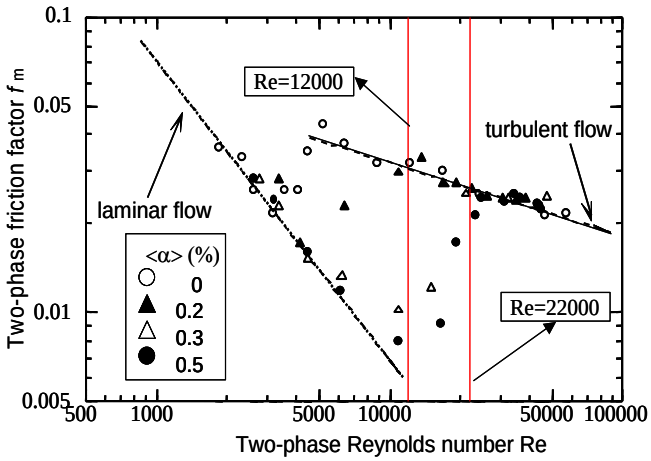

Figure 15 Measured Single- and Two-Phase Friction Factors

Laminar flow: $f_m = 64/\mathrm{Re}$ (17)

Turbulent flow: $f_m = 0.3164\,\mathrm{Re}^{-0.25}$ (18)

It has been confirmed that the single phase flow changed from laminar flow to turbulent flow at the Reynolds number Re = 2,300 ~ 2,500 as usually observed.

The most exciting and important finding in this work is evidence that the two-phase flow becomes laminarized by injecting micro bubbles into the water flow. For 0.3 ~ 0.5 % void fractions, the laminar-to-turbulent transition initiated at the Reynolds number Re = 10,000 ~ 12,000, as clearly indicated in Fig.15. It is also noted that the flow laminarization takes place even at such low void fraction as 0.2%. A similar flow laminarization has been reported to occur by an addition of either surfactant or polymer solution or fiber. The mechanism of flow laminarization which has been observed in the present work has not yet been clarified. However, we can find some statements as below which might be useful to pursue the mechanisms involved.

Marie [10] proposed an analytical model to explain the reduction of skin friction caused by small bubbles in the wall boundary layer. His conclusion is that micro bubbles are so small that they can penetrate into the buffer layer, affecting the turbulence in the buffer layer, and thus causing a change of certain physical properties of this layer. In practice, the drag reduction by bubble injection has been a topic for shipbuilders. Usually this type of researches has been conducted by using normal sized air bubbles instead of "real micro bubbles". A significant drag reduction has been reported so far. But the mechanism has not been clarified yet. We carried out a similar experiment for drag reduction using a model ship (2400mm long, 400mm wide acrylic boat) and "real micro bubble" injection with a cavitation nozzle similar to that used in the present experiment (Fig.16). Results indicated no reduction in drag coefficient caused by micro bubble injection, but up to roughly 5% reduction in drag coefficient was brought about by much larger air bubbles (approximately a few mm ~ 10 mm in diameter) at ship velocities even lower than 1.4 m/s (Serizawa et al.[11]).

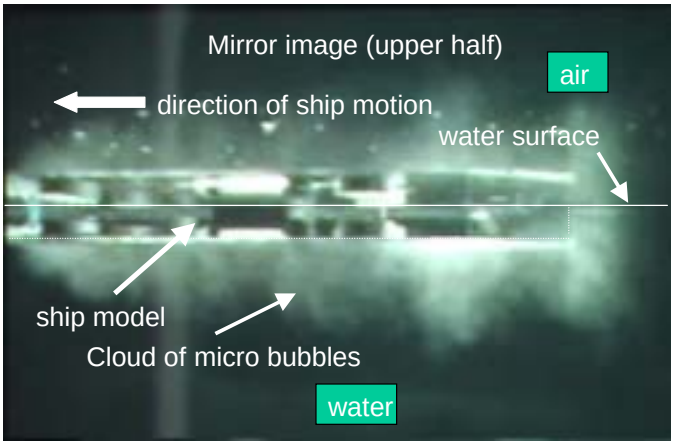

Figure 16 Drag Reduction Experiment using a Model Ship in Water Pool [11]

Another statement comes from the work by Rashidi et al.[12]. It is well known that when the shear rate is increased in a boundary layer near the wall, high speed and low speed regions alternately appear near the boundary. This low-speed/high-speed flow pattern results from counter-rotating streamwise vortex pairs that are broken up periodically near the wall, thus initiating bursting process. This bursting process is a randomly occurring event consisting of a gradual local liftup of low-speed streaks, sudden oscillation and ejection of low-momentum fluid from the wall region into main stream. This is then followed by a sweep of high-momentum fluid into the wall region. This bursting phenomenon was shown to be responsible for most of turbulence energy production and to be the major contribution to the transport of Reynolds stresses. Their particle-laden fluid experiments and visual observation showed that the particles can penetrate into the viscous sublayer because of their small size and large momentum, and they tend to accumulate in the low-speed streaks of the wall structures, as shown in Fig.17. These particles are then lift up (depending on their size and density) by the inclined vortex-loops of the wall region and are ejected into the bulk flow. Therefore, the frequency of the wall ejection and the streak velocities are influenced by particle loading. Rashidi et al. observed that the large particles (1100 μm polystyrene particles) caused an increase of the number of wall ejections and enhanced turbulence intensities and Reynolds stresses. On the other hand, the smaller polystyrene particles (~120 μm) caused a decrease in the frequency of wall ejection, giving lower turbulence intensities and Reynolds stresses. This effect is reported to have been enhanced as particle loading was increased. Although the micro air bubbles have much smaller momentum compared to the solid particles, micro bubbles injection into the water flow may affect the processes of sweep and ejections.

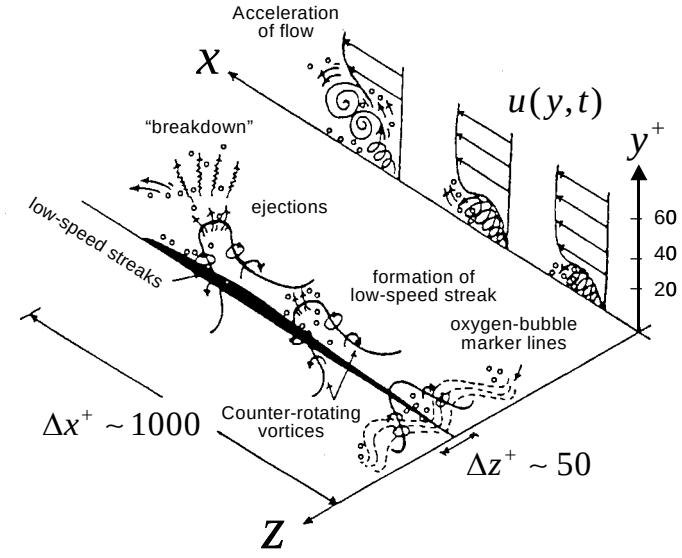

Fig.17 Mechanism of Ejection and Particle Transport near the Wall (Rashidi et.al.[12])

4.3 Liquid velocity

Laser Doppler anemometry and hot film anemometry are typical and powerful tools to measure local liquid velocity in gas-liquid two-phase bubbly flow. However both of these techniques are not available for micro bubbles containing milky bubbly flow. Firstly, the micro bubbles containing milky

bubbly flow is not optically transparent because of very high bubble number density (10^5 ~ a few mega bubbles/cc). Secondly, the two-phase mixture contains so small bubbles that the hot film sensor is easy to be covered by such bubbles attached onto the sensor, yielding to an unstable and fabulous operation. We therefore decided to use a very classical method, that is, a Pitot tube based on a continuous squeeze model expressed by Eq.(9)

Figures 18 and 19 show liquid velocity profiles in radial direction for single-phase and two-phase milky bubbly flows at the Reynolds number = 12,000 and 22,000, respectively. These values of the Reynolds number are indicated with solid lines in Fig.15 just for reference. By recalling that, in milky bubbly two-phase flow cases, the laminar-to-turbulent transition occurred roughly at Re ≈ 11,000 for α = 0.3% and α = 0.5%, Re = 12,000 corresponds to nearly laminar flow condition and Re = 22,000 corresponds to almost turbulent. As can be noticed from these figures, the single–phase water flow follows the 1/7 power law at both Reynolds numbers. On the other hand, in milky bubbly two-phase flow cases, i.e., α = 0.3% and α = 0.5%, there is a slightly different trend observed between the two Reynolds number cases. At Re = 12,000, the liquid velocity profiles become slightly flattened with being decelerated in the center portion of the tube and being accelerated in the wall region. This trend agrees with the experimental tendency observed in air-water bubbly flow consisting of ordinary sized bubbles (2 ~ 5 mm in diameter) (Serizawa et al. [13, 14]). On the other hand at Re = 22,000, the liquid velocity profile does not change for different void fraction $\langle\alpha\rangle$ but follows the 1/7-power law.

These observed trends in liquid velocity profiles are not inconsistent with the arguments about the $\langle\alpha\rangle$ *versus* β diagram described in section **4.1**. This speculation leads to a hypothesis that micro bubbles may collect to the center portion of the flow passage where the liquid velocity is high. This

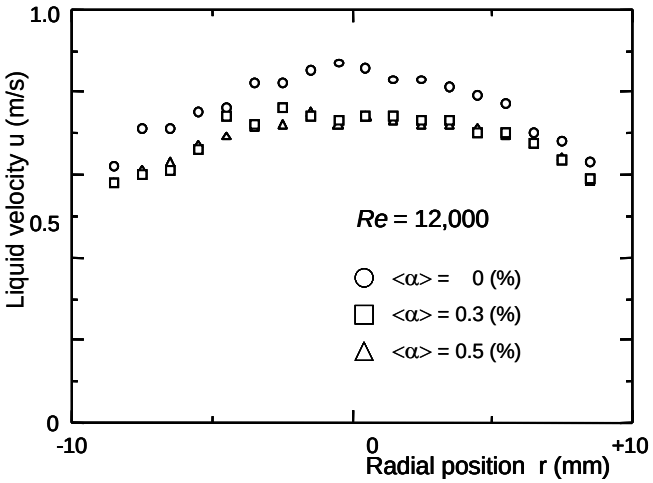

Figure 18 Liquid Velocity Profiles at Re = 12,000

hypothesis meets the requirement for high slip ratio S = 1.4. In order to confirm the validity of this hypothesis, the local void fraction measurement should be preferably conducted. However, this measurement is not an easy job at the moment due to a lack of precise measurement techniques. We are now trying to develop a method using a sampling tube, but we have not reliable data yet.

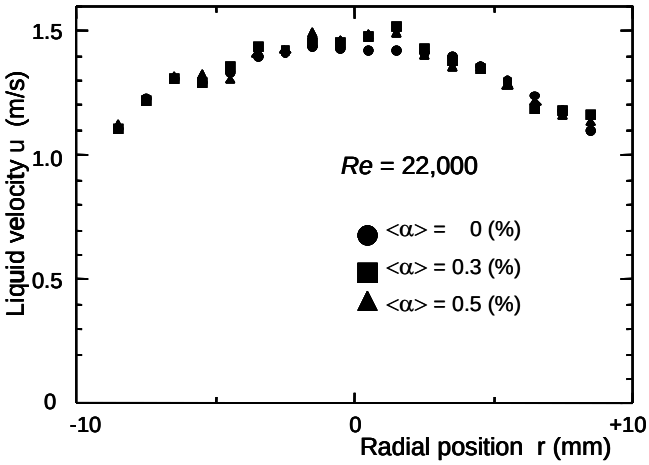

Figure 19 Liquid Velocity Profiles at Re = 22,000

4. CONCLUSIONS

We successfully realized a vertically upward micro bubbles containing milky bubbly two-phase flow in a 4m long, 20 mm ID transparent acrylic tube. This air-water two-phase test loop is equipped with a high performance micro bubble generating nozzle specially designed and developed in collaboration with Aura Jet Co. Ltd. This device generates micro bubbles with mean bubble diameter~ 40 μm and bubble number density higher than 2×10^5 bubbles/ cm^3. The maximum cross-sectional average void fraction attained was about 0.6 %, which is large enough to realize milky bubbly two-phase flow.

In view of small bubble sizes compared with micro turbulence scales in two-phase bubbly flow, we anticipate different bubble-bubble interactions and bubble-turbulence eddies interaction from those reported in earlier works about normal sized bubbles, i.e., bubbles with 1 ~ 5 mm in diameter, and hence different flow structures.

We measured cross-sectional average void fraction, two-phase frictional pressure drop and local liquid velocity profiles. The following conclusions have been drawn from the present work.

(1) The measured cross-sectional void fraction was correlated by the following empirical equation:

$$\langle\alpha\rangle = 0.702\beta$$

This result is not necessarily consistent with our intuition that the flow is rather homogeneous with negligibly small slip in macroscopic character between the two phases. The reason for this result has been discussed based on a drift flux model and measured local liquid velocity profiles. This speculation suggests non-uniform local void fraction distribution in the flow channel. However this should be confirmed and verified by experiment.

(2) Two-phase frictional pressure drop measurement clearly exhibits the flow laminarization by injecting micro bubbles into the water flow. This laminarization occurred at cross sectional void fractions larger than 0.2%. Although the mechanisms for this phenomenon have not been made clear yet, we think this is a very exciting and important finding with respect to the enhancement of our current understanding of physics in bubble-turbulence interactions in bubbly two-phase flow. This finding should

be expected to be extended to new applications in micro bubble technology as a functional or smart fluid.

(3) The local liquid velocity in milky bubbly flow follows nearly a 1/7-power law at high Reynolds numbers in turbulent flow, and a little bit flattened profile in radial direction at lower Reynolds numbers in near laminar flow. However, neither parabolic nor near-parabolic profiles have been observed under the flow conditioned covered in the present

NOMENCLATURES

C_o	distribution parameter
C_1, C_2	constants
D	tube diameter
F_B	bubble-bubble interaction force
F_m	volume fraction of m-th phase
f_m	friction factor
F_v	nominal surface tension force
$F_{v,total}$	total surface tension force
j	volumetric flux
L	distance between two adjacent bubbles
l	distance between pressure taps
m, n	constants
n	unit vector normal to surface
P	pressure
ΔP	pressure difference
ΔP_f	frictional pressure drop
R	tube radius
r	radial coordinate
R_b	bubble diameter
R_e	Reynolds number ($= \rho j_L D/\mu$)
u	velocity
(x,y,z)	coordinate system
x_s	surface position

Greeks and operators

α	local void fraction
β	volumetric gas flow ratio ($= j_G/(j_L+j_G)$)
κ	surface curvature
Λ	macro scale of turbulence
λ	micro scale of turbulence
μ	viscosity
ρ	density
σ	surface tension
τ	shear stress
$< >$	area-averaging

Suffix

L, G	liquid and gas phases
l, g	longitudinal and lateral direction, respectively
c, w	tube center and tube wall

REFERENCES

1. Michiyoshi, I, and Serizawa, A., 1986, Turbulence in two-phase bubbly flow, *Nuclear Engineering and Design*, Vol.95, pp.253-267.
2. Serizawa, A, and Kataoka, I., 1987, Phase distribution in two-phase flow, in *Transient phenomena in Multiphase Flow*, edited by N.H. Afgan, Hemisphere Pub.Co., N.Y., pp.179-224.
3. Fukami, T., 2002, A study of hydro-dynamic character-istics of multiphase flow with micro bubbles, Master thesis, Kyoto University (in Japanese)
4. Matsumoto, Y.,Fukami, T., Kunugi, T. and Serizawa, A., 2001, Fluid-Dynamic Structure of Air-Water Bubbly Flow with Micro-Bubbles, *Proc. Of the 4th International Conference on Multiphase Flow(ICMF-2001)*, New Orleans, LA, USA, Paper No.332 (in CD-ROM).
5. Brackbill, J.U., Kothe, D.B. and Zemach, C., 1992, *J. Comput. Phys.*, Vol.100, pp.335-344.
6. Kunugi, T., 1997, Direct numerical algorithm for multiphase flows with free surfaces and interfaces, *Trans. JSME, Ser.B.*, No.63, pp.1576-1584.
7. Serizawa, A. and Yahiro, T., 2001, Micro bubble nozzles and their operation, *Proc. of the Annual Meeting of the Japanese Society for Multiphase Flow*.
8 Machiya, K., et al., 1994, Production of bubbly water and its applications, *IDEC REVIEW*, Izumi Electric Co. Ltd., (in Japanese)
9 Serizawa, A., 2003, New aspect of two-phase flow – Application of Micro bubbles and its physics, Orally presented at t*he 5th UK-Japan Seminar on Multiphase Flow*, April, 2003, Surrey University, Surrey, UK.
10 Marie, J.L., 1987, Modeling of skin friction and heat transfer in turbulent two-component bubbly flow in pipes, *Int. J. Multiphase Flow*, Vol.13, No.3**,** pp.309-325.
11 Serizawa, A., 2003, A study on drag reduction with micro bubble injection nozzle for application to ships, R*eport of the Activities from Joint Research Projects*, Research Institute of Applied Mechanics, Kyushu University (in Japanese).
12 Rashidi, M., Hetsroni, G. and Banerjee, S., 1990, Particle-turbulence interaction in a boundary layer, *Int. J. Multiphase Flow*, Vol.16, No.6**,** pp.935-949.
13 A. Serizawa, 1974, Fluid Dynamic Characteristics of Two-Phase Flow, Dissertation, Kyoto University.
14 Serizawa, A., Kataoka, I. and Michiyoshi, I., 1975, Turbulence structure of air-water bubbly flow – II. Local properties, *Int. J. Multiphase Flow*, Vol.2, pp.235-246.